Elliptic Stochastic Fields in Reverberation Chambers

Luk R. Arnaut, *Senior Member, IEEE*

***Abstract*—A theoretical and experimental characterization of complex elliptic random fields inside a reverberation chamber is performed. The real and imaginary parts of the pseudovariance and noncircularity quotient are found to be simultaneously nonzero and to have comparable magnitudes, in general. The I/Q statistical anisotropy and correlation have a spectral envelope that is robust under varying experimental conditions and decays at -5 dB per decade, on average. Expansion coefficients for a circular random base field are extracted for a widely linear field representation. Joint, marginal and conditional probability density functions are derived for both the unconditional and the directional energy and for the phase. An iterative stochastic algorithm is developed for the systematic extraction of the sampling distributions. These distributions provide increased model accuracy and improved agreement with empirical distributions, provided the constellation of sample stir data conforms to a symmetric complex elliptic distribution.**

***Index Terms*—Complex elliptic distribution, random field, reverberation chambers, stochastic modeling.**

I. Introduction

In the characterization of dynamic complex electromagnetic (EM) environments based on stochastic methods, first-order probabilistic [1], [2] and second-order spectral [3], [4] density functions are essential tools. In EMC, these enable the statistical quantification of system reliability, immunity, risk, and safety. In particular, accurate models for the probability density functions (PDFs) are needed for estimating the probability of failure, uncertainty quantification based on propagation of probability, confidence intervals, extreme-value distributions, etc.

The usual working assumption in modeling random EM fields is that of *circularity*, i.e., independent and identical distributed in-phase (I-) and quadrature (Q-) components of the complex-valued time-harmonic field phasor ($\exp(\mathrm{j}\omega t)$ time dependence assumed). For ideal Gaussian fields, circularity is equivalent to uncorrelated I/Q components with identical I/Q variances. Circularity leads to statistically homogeneous, isotropic, unpolarized, incoherent random fields [1], [3], [4]. Although statistical field anisotropy of Cartesian components and finite-sample effects have served as useful departures for realistic random fields, the effect of noncircularity on the distribution of field magnitude, power, and phase remains to be investigated generally and systematically, which is the subject of this paper. Explicit results for several special cases were reported in [5].

Manuscript received April 29, 2015; revised July 25, 2015; accepted September 9, 2015. Date of publication December 1, 2015; date of current version February 16, 2016.

L. R. Arnaut is with the Laboratory of Stochastic Electromagnetism and Wave Complexity, School of Electronic Engineering and Computer Science, Queen Mary University, London E1 4FZ, U.K. (e-mail: l.arnaut@qmul.ac.uk).

Color versions of one or more of the figures in this paper are available online at http://ieeexplore.ieee.org.

Digital Object Identifier 10.1109/TEMC.2015.2482976

In the context of EMC, mode-tuned and mode-stirred reverberation chambers (MT/MSRCs) offer an environment for studying quasi-static or dynamic random fields, respectively. In overmoded conditions, modeled by an angular spectrum of random plane waves, circularity arises are a result of the local incoherent superposition of multiple reflected waves whose range of phase differences is well in excess of 2π. Thus, even an initially linearly polarized CW excitation field (I-component) rapidly tends toward circularity (I/Q balance) at the receiving antenna because of 1) a large number of reflections and 2) path length differences in excess of the wavelength. While a large number of reflections is essential in order to make statistical modeling feasible, differences in path lengths can be limited, resulting in an imperfect mixing (randomization) of the reflected field and a smaller spread among Q- compared to I-fields.

While the exposition in this paper focuses on the EM field, the methods also apply to other complex-valued stochastic EM quantities, e.g., current, permittivity, conductance, wavenumber, near-field energy or power, etc. Moreover, in wireless communications, noncircularity also arises in certain digital modulation schemes (BPSK, PAM, etc.). Precise knowledge of their statistics is important to optimize the transmission.

II. Theory

A. Complex Elliptic Field

For later use, we briefly review and extend some definitions relating to noncircularity.

1) Definitions: Let E' and E'' denote the I- and Q- components of a complex-valued random electric field $E \equiv E' + \mathrm{j}E''$ at frequency f with complex conjugate E^*. Second-order properties of E are governed by its (real) variance

$$\sigma_E^2 \stackrel{\Delta}{=} \langle (E - \langle E \rangle)(E - \langle E \rangle)^* \rangle = \sigma_{E'}^2 + \sigma_{E''}^2 \tag{1}$$

and its (complex) pseudovariance $\tau_E \equiv \tau_E' + \mathrm{j}\tau_E''$ [6], [7]

$$\tau_E \stackrel{\Delta}{=} \langle (E - \langle E \rangle)^2 \rangle = \sigma_{E'}^2 - \sigma_{E''}^2 + \mathrm{j}2\sigma_{E',E''} \tag{2}$$

with $\rho_{E',E''} \stackrel{\Delta}{=} \sigma_{E',E''}/(\sigma_{E'}\sigma_{E''})$ obtained as the (real) I/Q correlation coefficient. For second-order circular random fields, I and Q are statistically balanced ($\sigma_{E'}^2 = \sigma_{E''}^2$) and uncorrelated ($\rho_{E',E''} = 0$), whence $\tau_E = 0$. In this case, the second-order properties of E are solely governed by its variance.

The noncircularity quotient $\varrho_E \equiv \varrho_E' + \mathrm{j}\varrho_E''$ is the correlation coefficient between E and E^* [8]. From (1) and (2), we obtain

$$\varrho_E \stackrel{\Delta}{=} \rho_{E,E^*} = \frac{\tau_E}{\sigma_E^2} \tag{3}$$

$$= \frac{\sigma_{E'}^2 - \sigma_{E''}^2}{\sigma_{E'}^2 + \sigma_{E''}^2} + \mathrm{j}\left[\frac{1}{2}\left(\frac{\sigma_{E'}}{\sigma_{E''}} + \frac{\sigma_{E''}}{\sigma_{E'}}\right)\right]^{-1} \rho_{E',E''} \tag{4}$$

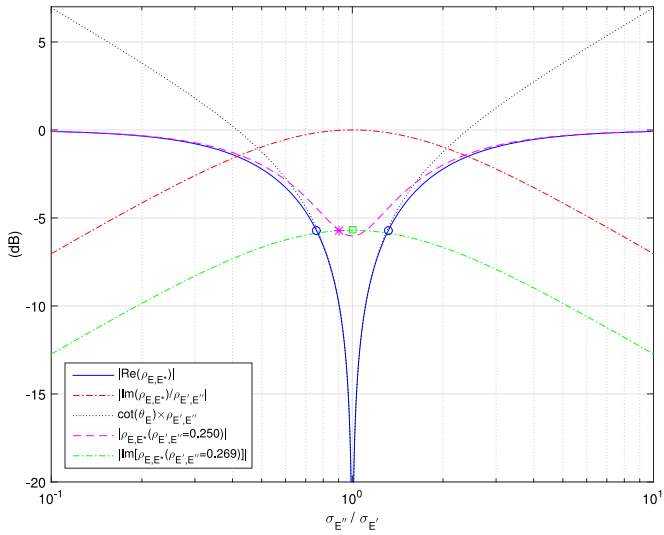

Fig. 1. Contributions to ϱ_E as a function of $\sigma_{E''}/\sigma_{E'}$. The equal ordinate values of the points indicated by the symbols demonstrate that I/Q anisotropy and I/Q correlation are exchangeable.

i.e., a function of $\sigma_{E''}/\sigma_{E'}$ [9] and $\rho_{E',E''}$. The real part ϱ'_E measures the statistical I/Q anisotropy, i.e., the difference between the spreads of I- and Q-fluctuations relative to their overall (combined) variance [11], whereas ϱ''_E depends on both the I/Q correlation and the imbalance $\sigma_{E''}/\sigma_{E'}$. In quantum electrodynamics, ϱ_E is known as the phase rigidity [12].

The tangent of the correlation angle ϑ_E, i.e.,

$$\tan\vartheta_E \triangleq \frac{\tau''_E}{\tau'_E} = \left[\frac{1}{2}\left(\frac{\sigma_{E'}}{\sigma_{E''}} - \frac{\sigma_{E''}}{\sigma_{E'}}\right)\right]^{-1} \rho_{E',E''} \tag{5}$$

measures the I/Q correlation relative to the I/Q anisotropy. Note that statistical planar field anisotropy and mutual correlation as in (4) for the intensities of two Cartesian *spatially* orthogonal fields was previously studied in [10] and [11, Section 5.2]. Here, the focus is instead on electrically orthogonal I- and Q-components, for a single spatial direction.

Fig. 1 shows the dependencies of $|\varrho'_E|$, $|\varrho''_E/\rho_{E',E''}|$, $\rho_{E',E''}\cot\vartheta_E$, and $|\varrho_E|$ on $\sigma_{E''}/\sigma_{E'}$, the latter for $\rho_{E',E''} = 0.25$. One effect of nonzero $\rho_{E',E''}$ is the reduced sensitivity (slope) of $|\varrho_E(\sigma_{E''}/\sigma_{E'})|$ compared to $\varrho'_E(\sigma_{E''}/\sigma_{E'})$, particularly near I/Q balance ($\sigma_{E''}/\sigma_{E'} = 1$). When $\rho_{E',E''} = 1$, this variation is completely eliminated ($|\varrho_E| = 1$, $\forall\sigma_{E''}/\sigma_{E'}$). Furthermore, $|\varrho_E|$ increases with $|\rho_{E',E''}|$, for arbitrary $\sigma_{E''}/\sigma_{E'}$. This can be conceived as an effective shift of $\sigma_{E''}/\sigma_{E'}$ toward 1 for constant $|\varrho_E|$. For example, for $\rho_{E',E''} = 0$ (i.e., $|\varrho_E| \equiv \varrho'_E$), choosing $\sigma_{E''}/\sigma_{E'} = 0.775^{\pm 1}$ yields $|\varrho_E| = -6.02$ dB, which is also obtained for $\rho_{E',E''} = 0.25$ when $\sigma_{E''} = \sigma_{E'}$. More generally, for any $(\varrho'_E, \varrho''_E) \neq (0,0)$, e.g., when $(\sigma_{E''}/\sigma_{E'}, \rho_{E',E''}) = (0.902, 0.254) \neq (1,0)$, one can exchange this pair for $(0.759^{\pm 1}, 0)$ or $(1, 0.269)$ while maintaining $|\varrho_E| = -5.70$ dB (see symbols in the figure). Thus, statistical I/Q anisotropy and I/Q correlation are fully exchangeable for arbitrary $|\varrho_E|$. This aspect will be important in the interpretation and implications of (10) in Section II-B1.

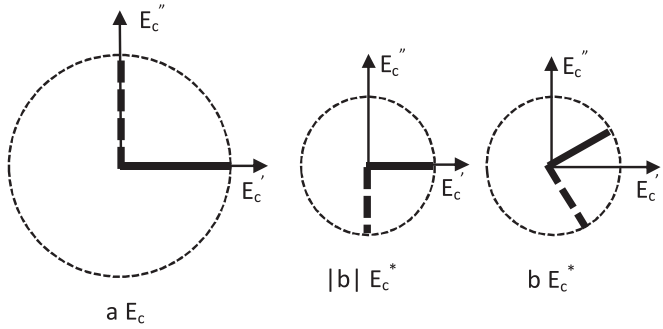

Fig. 2. Components aE_c and bE_c^* of the WL expansion (6) for $E - \mu_E$. Mutually perpendicular solid and dashed lines represent in-phase and quadrature components of E_c, respectively (left figure), which are then mirrored to E_c^* and scaled in length by $|b|/a$ (middle figure), followed by rotation by $\arg(b)$ (right figure).

2) Widely Linear (WL) Composition: The ellipticity of an arbitrary random field E can be regarded as a perturbation to its ideal circularity. Consider a zero-mean circular complex random field $E_c = E'_c + \mathrm{j}E''_c$, which may be Gaussian or other. Its I- and Q-components can be individually scaled by different (real) factors c_R and c_I to yield the linear composition $E = \mu_E + c_R E'_c + \mathrm{j}c_I E''_c$. The WL representation of E is, for complex a, b [13] (see Fig. 2)

$$E = \mu_E + aE_c + bE_c^*. \tag{6}$$

In particular, E_c can be standardized to a unit base field $E_{c,0}$ (i.e., $\mu_{E_{c,0}} = 0$, $\sigma_{E_{c,0}} \equiv \sqrt{2}\sigma_{E'_{c,0}} = \sqrt{2}\sigma_{E''_{c,0}} \triangleq 1$, $\rho_{E'_{c,0},E''_{c,0}} = 0$). Choosing $a = 1$ thus results in

$$E = \mu_E + \sigma_{E_c}\left(E_{c,0} + \frac{b}{\sigma_{E_c}}E_{c,0}^*\right). \tag{7}$$

As such, $(b/\sigma_{E_c})(E_{c,0}^*/E_{c,0})$ defines a complex fractional change to $E_{c,0}$ that yields E. With the variance $\sigma_E^2 = \sigma_{E_c}^2 + |b|^2$ and pseudovariance $\tau_E = 2\sigma_{E_c} b$ for a specified (i.e., measured) E, these yield three scalar equations, from which the model parameters (b', b'', σ_{E_c}) follow as

$$b' = \frac{\tau'_E}{2\sigma_{E_c}}, b'' = \frac{\tau''_E}{2\sigma_{E_c}}, \sigma_{E_c} = \frac{\sigma_E}{\sqrt{2}}\sqrt{1 + \sqrt{1 - \frac{|\tau_E|^2}{\sigma_E^4}}} \tag{8}$$

whence, with (4), $\lim_{\tau_E/\sigma_E^2 \to 0}(b/\sigma_{E_c}) = \varrho_E/2$.

The merit of the WL representation for noncircular E lies in the fact that methods and theorems for time-harmonic random circular EM fields and currents can be easily extended to elliptic fields (modulated or randomized) by an appropriate linear combination of a circular phasor and its complex conjugate. Thus, the phasor representation of $E = |E|\exp(\mathrm{j}\phi)$ becomes

$$\begin{aligned}\mathrm{Re}[E\exp(\mathrm{j}\omega t)] = {} & \mathrm{Re}[|a||E_c|\exp(\mathrm{j}\omega t + \phi_c + \phi_a)] \\ & + \mathrm{Re}[|b||E_c|\exp(\mathrm{j}\omega t - \phi_c + \phi_b)].\end{aligned} \tag{9}$$

B. Intensity, Energy, and Power

1) Ensemble Distributions: The stochastic representation and generation of PDFs for multidimensional elliptic

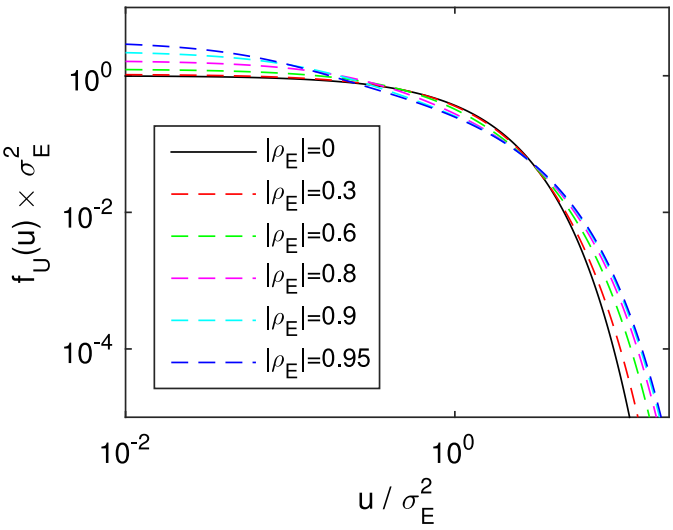

Fig. 3. PDF $f_U(u)$ for intensity of elliptic field $U = |E|^2$, for selected values of $|\varrho_E|$.

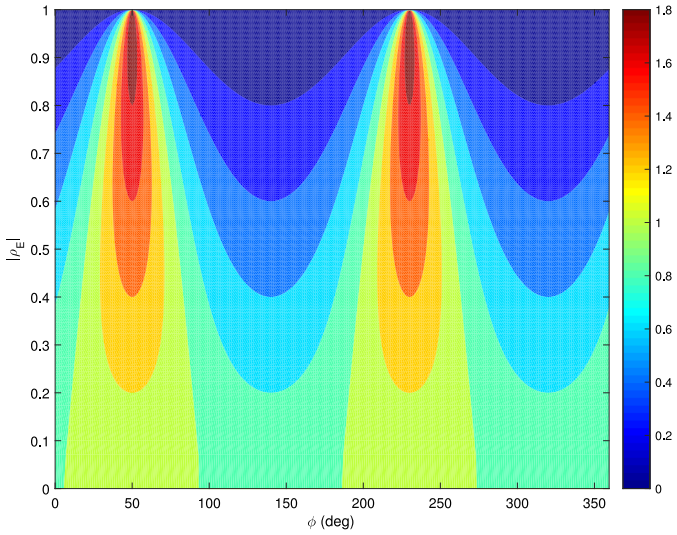

Fig. 4. Contour plot of $\sigma_{U|\Phi}/\sigma_E^2$ for $\vartheta_E = 100°$ as a function of $|\varrho_E|$ and ϕ.

random fields is detailed in the appendix. There, it is shown using complex stochastic calculus that for a 2-D elliptic Gaussian E, the ensemble PDFs of the intensity (normalized energy) $U \equiv |E|^2 = E'^2 + E''^2 \triangleq U' + U''$ and phase angle $\Phi \triangleq \tan^{-1}(E''/E')$ are

$$f_U(u) = \frac{\exp\left[-\frac{u}{\sigma_E^2(1-|\varrho_E|^2)}\right]}{\sigma_E^2\sqrt{1-|\varrho_E|^2}} I_0\left(\frac{|\varrho_E|}{\sigma_E^2(1-|\varrho_E|^2)}u\right) \quad (10)$$

$$f_\Phi(\phi) = \frac{\sqrt{1-|\varrho_E|^2}}{2\pi[1-|\varrho_E|\cos(2\phi-\vartheta_E)]} \quad (11)$$

for $0 \le u < +\infty$ and $-\pi \le \phi < +\pi$, respectively.

Fig. 3 shows (10) for selected $|\varrho_E|$. Increasing $|\varrho_E|$ increases the kurtosis, including a heavier tail. The latter is of particular importance for characterizing extreme values in EMC (immunity and emissions testing) and in wireless communications (fading). The phase PDF $f_\Phi(\phi)$ exhibits oscillatory nonuniformity that increases with $|\varrho_E|$, manifesting itself in two peaks centered at $\phi = \vartheta_E/2$ and $\vartheta_E/2 + \pi$, signifying an increased concentration of scattered data near the major axis of the concentric ellipses of equiprobability density (with a consequent depletion near their minor axis). For circular fields ($\varrho_E = 0$), the well-known negative exponential (χ_2^2) PDF for U and associated uniform PDF for Φ [1] are retrieved as special cases of (10) and (11).

The discussion of Fig. 1 now applies to the dependence of $f_U(u)$ on $|\varrho_E|$: the case of nonzero I/Q correlation $\rho_{E',E''}$ with an arbitrary $\sigma_{E''}/\sigma_{E'}$ (see purple asterisk in Fig. 1) can be exchanged for either one of the two points with vanishing $\rho_{E',E''}$ but different $\sigma_{E''}/\sigma_{E'}$ (blue circles), while still achieving the same $|\varrho_E|$ and, hence, $f_U(u)$. Conversely, $\varrho'_E = 0$ can be made to vanish ($\sigma_{E''} = \sigma_{E'}$) while increasing $\rho_{E',E''}$ to the same effect (green square).

Unlike for circular fields, the PDF of the full energy of an elliptic field based on a particular selected I/Q direction (phase) ϕ is no longer independent of ϕ, viz.,

$$f_{U|\Phi}(u|\phi) = \frac{f_{U,\Phi}(u,\phi)}{f_\Phi(\phi)} = \frac{1-|\varrho_E|\cos(2\phi-\vartheta_E)}{\sigma_E^2(1-|\varrho_E|^2)} \times \exp\left[-\frac{1-|\varrho_E|\cos(2\phi-\vartheta_E)}{\sigma_E^2(1-|\varrho_E|^2)}u\right] \quad (12)$$

i.e., a χ_2^2 PDF with a rescaled standard deviation

$$\sigma_{U|\Phi} = \frac{1-|\varrho_E|^2}{1-|\varrho_E|\cos(2\phi-\vartheta_E)}\sigma_E^2 \quad (13)$$

that depends on the direction ϕ of cutting the joint PDF "cloak" $f_{U,\Phi}$, whose ellipses of equiprobability density have an orientation and aspect ratio that depend on ϱ_E. As an example, the dependencies of $\sigma_{U|\Phi}/\sigma_E^2$ on $|\varrho_E|$ and ϕ for $\vartheta_E = 100°$ and $\sigma_E^2 \equiv \sigma_U(\varrho_E = 0)$ are shown in Fig. 4.

As an engineering application, the PDF (12) is relevant in I/Q demodulation of quasi-stochastic communication signals, e.g., for COFDM, where guard intervals contain decaying echoes. The interval length must be sufficiently long in order to avoid intersymbol interference, whose level is a function of the echo intensity. To this end, the maximum echo delay time for the COFDM signal must be determined, requiring accurate knowledge of $f_U(u)$. The transmission can be emulated and assessed using, e.g., a vector modulation analyzer [14]. In detection problems, variates that depend on multiple values of Φ are of interest, e.g., for the ratio $(U_1|\Phi = \phi_1)/(U_2|\Phi = \phi_1 + \pi/2)$ for two perpendicular directions in the I/Q plane, which follows from (12) as a Fisher–Snedecor $F(2,2)$ variate.

Conversely, and again unlike for circular fields, the I/Q phase can be estimated conditional-probabilistically from the energy

based on

$$f_{\Phi|U}(\phi|u) = \frac{f_{U,\Phi}(u,\phi)}{f_U(u)} = \left[\pi I_0\left(\frac{|\varrho_E|u}{\sigma_E^2(1-|\varrho_E|^2)}\right)\right]^{-1} \times \exp\left\{\frac{|\varrho_E|u}{\sigma_E^2(1-|\varrho_E|^2)}\cos[2\phi-\vartheta_E]\right\}. \quad (14)$$

For the amplitude (envelope) $A \equiv |E| \propto \sqrt{U}$, the PDF follows from (37) as $f_A(a) = 2a f_U(a^2)$, i.e.,

$$f_A(a) = \frac{2a\,\exp\left[-\frac{a^2}{\sigma_E^2(1-|\varrho_E|^2)}\right]}{\sigma_E^2\sqrt{1-|\varrho_E|^2}} I_0\left(\frac{|\varrho_E|}{\sigma_E^2(1-|\varrho_E|^2)}a^2\right). \quad (15)$$

Note that (15) differs from a Nakagami–Rice PDF for a constant biasing phasor plus random circular phasor—in the present context, a line-of-sight (unstirred) field plus ideal reverberant (multipath) field—in that the argument of $I_0(\cdot)$ is proportional to a^2 rather than a. Both PDFs can be merged, formally,[1] by "randomizing the bias" in replacing it with $a|\varrho_E|/2$, in conjunction with reducing the (circular) variance σ_E^2 to $\sigma_E^2(1-|\varrho_E|^2)$. For the contribution of ϱ_E', this is easily understood from (2) because "stretching" the marginal PDF for I or Q produces a phase bias in the randomization. For $\varrho_E'' \propto \rho_{E',E''}$, which is symmetric in I and Q, this may seem less obvious. However, recall that a purely imaginary ϱ_E causes a stretch of the joint PDF along the bisector $E' = E''$ in the I/Q plane in order to maintain $\sigma_{E'} = \sigma_{E''}$, causing a bias for the probability density for this direction.

For the directional I-energy U' (or, similarly, the Q-energy U''), its PDF follows from (30) with [15, eq. (3.323.2)] as

$$f_{U'}(u') = \frac{\exp\left[-\frac{u'}{2(1-\rho^2_{E',E''})\sigma^2_{E'}}\right]}{4\pi\sigma_{E'}\sigma_{E''}\sqrt{1-\rho^2_{E',E''}}\sqrt{u'}} \times \int_{-\infty}^{+\infty}\exp\left[\frac{2\rho_{E',E''}\sigma_{E''}\sqrt{u'}x - \sigma_{E'}x^2}{2(1-\rho^2_{E',E''})\sigma_{E'}\sigma^2_{E''}}\right]\mathrm{d}x = \frac{1}{2\sqrt{2\pi\sigma^2_{E'}}}\frac{\exp\left[-\frac{u'}{2\sigma^2_{E'}}\right]}{\sqrt{u'}} \quad (16)$$

i.e., a χ_1^2 PDF, independent of $\sigma^2_{E''}$ and $\rho_{E',E''}$. The corresponding I-amplitude A' exhibits a semi-Gaussian χ_1 PDF $f_{A'}(a') = (1/a')\exp[-a'^2/(2\sigma^2_{E'})]/\sqrt{2\pi\sigma^2_{E'}}$.

2) Sampling Distributions: The PDFs (10) and (11) represent *ensemble* densities, containing $\sigma_{E'^{(\prime)}}$ and $\rho_{E',E''}$ as deterministic parameters with assumed known values. For statistically inhomogeneous fields, these parameters are themselves subject to uncertainty or fluctuations (e.g., as a function of antenna location/orientation). This necessitates the use of sampling PDFs with the number of degrees of freedom (NDoF) (effective sample size) N as a distribution parameter.

Ensemble PDFs of a complex normal *circular* E yield Bessel K sampling PDFs for dimensioned E, $|E|$, and $|E|^2$ [16]. In particular, Bessel K PDFs of order $p = 1/2$ represent sampling PDFs for an individual normal I- or Q-component $|E'^{(\prime)}|^2$ with an ensemble χ_1^2 PDF. In [17], it was demonstrated that such *sampling* PDFs—despite corresponding to the simplest (viz., circular normal) PDF for ensemble E—can yield closer agreement with the empirical distribution of $|E|^2$, compared to the agreement with Bessel I *ensemble* distributions, even though the latter originate from a more sophisticated complex elliptic normal PDF of E. Whether a Bessel K (sampling) PDF for circular E offers better agreement with an empirical PDF than a (ensemble) Bessel I PDF for elliptic E for a particular dataset depends on 1) the NDoF because a relatively low value allows for matching heavier tails, and 2) $|\varrho_E|$ being not too close to 1, in order that the model ensemble PDF is not oversimplified. Indeed, [17, Fig. 3] has shown that these different aspects may lead to better agreement with either Bessel K PDFs (for $|E_x|^2$ and $|E_y|^2$) or Bessel I PDFs (for $|E_z|^2$).

Naturally, *sampling* distributions for an *elliptic* ensemble E, associated with (37) and (39), are expected to offer superior agreement with measured data in any case. Such agreement is of course in the mean, particularly at lower frequencies and in the tails of the PDF, where ensemble distributions typically exhibit poorer correspondence.

a) *Incoherent Detection (Scalar Measurement):* In (phaseless) square-law detection, the sampling PDFs of $U \propto |E|^2$ and Φ can be calculated from their ensemble PDFs by considering the latter as conditional ones for supplementary PDFs of the sample variance and the correlation coefficient as follows. Following [16], f_U follows as the marginal PDF[2]

$$f_U = \int\int f_{U,S_E^2,R_{E,E^*}}\mathrm{d}s_E^2\mathrm{d}r_{E,E^*} \quad (17)$$

where S_E^2 and R_{E,E^*} are the sampled σ_E^2 and $\rho_{E,E^*} \equiv \varrho_E$, respectively, and

$$f_{U,S_E^2,R_{E,E^*}} = f_{U|(S_E^2,R_{E,E^*})}\cdot f_{S_E^2,R_{E,E^*}} \quad (18)$$

is the (joint) total PDF of U, S_E^2, and R_{E,E^*}, while the conditional PDF of U is

$$f_{U|(S_E^2,R_{E,E^*})} = \frac{\exp\left[-\frac{u}{s_E^2(1-|r_{E,E^*}|^2)}\right]}{s_E^2\sqrt{1-|r_{E,E^*}|^2}} \times I_0\left(\frac{|r_{E,E^*}|}{s_E^2(1-|r_{E,E^*}|^2)}u\right). \quad (19)$$

If S_E^2 and R_{E,E^*} can be considered to be mutually independent, then their joint PDF $f_{S_E^2,R_{E,E^*}}$ follows as

$$f_{S_E^2,R_{E,E^*}} = f_{S_E^2}\cdot f_{R_{E,E^*}}. \quad (20)$$

[1]Note that this particular randomization is fully correlated with the circular field, as it is proportional to a. Hence the stated argument is a heuristic one, because a proper conditional PDF should be used.

[2]For simplicity of notation, we omit the argument of the PDFs if there is no possible confusion, i.e., $f_X \equiv f_X(x)$.

Denoting $S_E^{(+)^2} \equiv S_E^2$ and $S_E^{(-)^2} \equiv T_E^2$ where $S_E^{(\pm)^2} \triangleq S_{E'}^2 \pm S_{E''}^2$, then both $f_{S_E^{(\pm)^2}}$ follow with [15, eq. (3.382.2)] as

$$f_{S_E^{(\pm)^2}} = \int_0^{s_E^{(\pm)^2}} f_{S_{E'}^2}(s_{E'}^2) \cdot f_{S_{E''}^2}(\pm(s_E^{(\pm)^2} - s_{E'}^2))\mathrm{d}s_{E'}^2$$

$$= c_{S_E^{(\pm)^2}} \cdot \left(s_E^{(\pm)^2}\right)^{\frac{N}{2}-1} \exp\left[\frac{(N-1)\gamma_E^{(\pm)}}{4} s_E^{(\pm)^2}\right]$$

$$\times I_{\frac{N}{2}-1}\left[\frac{(N-1)\gamma_E^{(\mp)}}{4} s_E^{(\pm)^2}\right] \quad (21)$$

in which $\gamma_E^{(\pm)} \triangleq \sigma_{E'}^{-2} \pm \sigma_{E''}^{-2}$, where $f_{S^2_{E'^{(\prime)}}}$ are scaled χ^2_{N-1} sampling PDFs obtained by variate transformation of [16, eqs. (8)–(10)] for $p = 1$ (i.e., [18, eq. (41)]), with normalization constants

$$c_{S_E^{(\pm)^2}} = \frac{\left(\frac{N-1}{2}\right)^{\frac{N}{2}} \Gamma\left(\frac{1}{2}\right)}{\Gamma\left(\frac{N-1}{2}\right)\left(\sigma_{E'}^2\sigma_{E''}^2\right)^{\frac{N-1}{2}} \left(\gamma_E^{(\mp)}\right)^{\frac{N}{2}-1}}. \quad (22)$$

The PDF of the sample circularity quotient R_{E,E^*}, i.e.,

$$R_{E,E^*} \triangleq \frac{T_E}{S_E^2} = \frac{S_{E'}^2 - S_{E''}^2}{S_{E'}^2 + S_{E''}^2} + \mathrm{j}\frac{R_{E',E''}}{S_{E'}^2 + S_{E''}^2} \quad (23)$$

follows by further variate transformations, assuming that the terms and factors constituting (23) are at least approximately independent and recalling the sampling PDF of the Pearson I/Q correlation coefficient [19]

$$f_{R_{E',E''}} = \frac{(N-2)\Gamma(N-1)(1-\rho_{E',E''}^2)^{\frac{N-1}{2}}}{\sqrt{2\pi}\Gamma(N-\frac{1}{2})}$$

$$\times \frac{(1-r_{E',E''}^2)^{\frac{N-1}{4}}}{(1-\rho_{E',E''}r_{E',E''})^{N-\frac{3}{2}}}$$

$$\times {}_2F_1\left(\frac{1}{2}, \frac{1}{2}; N-\frac{1}{2}; \frac{1+\rho_{E',E''}r_{E',E''}}{2}\right) \quad (24)$$

where ${}_2F_1(\cdot)$ represents a hypergeometric series [15, eq. (9.100)]. The sampling PDFs assume equal NDoFs N' for E' and N'' for E'' ($N' = N'' \triangleq N$). In practice, $N' \neq N''$ (cf., Section III-G) and one may define, e.g., $N = (N' + N'')/2$ or $\sqrt{N'N''}$. If the distribution parameters are not statistically independent, more appropriate PDFs $f_{S_E^2,R_{E,E^*}}$ are needed.

The sampling PDF of Φ follows in an analogous manner as

$$f_\Phi = \int f_{\Phi|R_{E,E^*}} \cdot f_{R_{E,E^*}} \mathrm{d}r_{E,E^*}. \quad (25)$$

Sampling distributions for the axial ratio and tilt (cf., Section III-E) of the equidensity ellipses for E can also be derived based on (21) and (24).

b) Coherent Detection (Vector Measurement): For a vector (I/Q-) detector, the sampling PDF for U can be based on individually measured I- and Q-components. Hence, it is obtained from the sampling joint PDF of E and E^*, followed by variate transformation to $|E|^2$ and Φ. The sampling PDF of E and E^* follows as the marginal PDF

$$f_{E,E^*} = \int\int f_{E,E^*,S_E^2,R_{E,E^*}} \mathrm{d}s_E^2 \mathrm{d}r_{E,E^*} \quad (26)$$

in which the joint PDF can be factorized as $f_{E,E^*,S_E^2,R_{E,E^*}} = f_{(E,E^*)|(S_E^2,R_{E,E^*})} \cdot f_{S_E^2,R_{E,E^*}}$. Subsequent expansions and calculations proceed similarly to the incoherent case.

III. Measurement Results

A. Measurement Configuration

Complex S-parameter data were measured in a $8.7 \times 3.7 \times 2.9$ m^3 mode-stirred reverberation chamber [20] (first resonance at $f_{110} \simeq 43.8$ MHz), from 40 MHz to 5.040 GHz with a 125-kHz sampling step, using a pair of identical log-periodic antennas ($M = 1000$ equiangular stir steps), and again from 100 MHz to 12 GHz, now with a 150-kHz sampling step using a pair of identical broadband dipole antennas (1400 stir steps). Although the antennas exhibit considerable impedance mismatch at the lowest and highest measurement frequencies over these wide bands, previous analysis has shown that this mismatch is of little significance in considering the ratios of S-parameter-based quantities [20], pertinent to the present analysis.

B. Variance, Pseudovariance, and Noncircularity

Fig. 5(a) shows $\sigma_{S_{21}}^2(f)$, $|\tau_{S_{21}}(f)|$, and $\varrho_{S_{21}}(f)$ for raw $S_{21}(f)$ data measured with the log-periodic antennas. The effect of any impedance mismatch on $|\tau_{S_{21}}(f)|$ and $\sigma_{S_{21}}^2(f)$ cancels in their ratio $\varrho_{S_{21}}$. Except for values close to unity at very low frequencies, the envelope of $|\varrho_{S_{21}}(f)|$ decays approximately as $f^{-1/4}$ (-5 dB/dec) above 200 MHz, asymptotically approaching ideal circularity ($|\varrho_{S_{21}}(f \to +\infty)| \to 0$). Compared with the net transmission $S_{21}^{(0)}(f) \triangleq S_{21}(f)/\{[1 - S_{11}(f)][1 - S_{22}(f)]\}$ [see Fig. 5(b)], the envelope $|\varrho_{S_{21}}(f)|$ is highly robust to such normalization. Compared to $|S_{21}|^2$ using the dipoles [see Fig. 5(c)], the slope but not the levels[3] of $|\varrho_{S_{21}}(f)|$ are maintained. Thus, $|\varrho_{S_{21}}(f)|$ is robust with respect to normalization and antenna type, but not to antenna position.

C. Relative Contributions of Anisotropy and Correlation to Noncircularity

1) Spectral Characteristics: To investigate the contributions to the noncircularity in more detail, absolute values of $\varrho'_{S_{21}}(f)$ and $\varrho''_{S_{21}}(f)$ are shown in Fig. 6(a). On average, both exhibit comparable magnitudes per frequency. Thus, statistical I/Q anisotropy and correlation in reverberation chambers should not be considered in isolation but are, in general, simultaneously nonzero. Moreover, both $\varrho'_{S_{21}}(f)$ and $\varrho''_{S_{21}}(f)$ fluctuate quasi-symmetrically across positive and negative values, on average

[3]The change of the average level between $|\varrho_{S_{21}}(f)|$ and $|\varrho_{S_{21}^{(0)}}(f)|$, and the relatively small step change in the envelope of $|\varrho_{S_{21}}(f)|$ at 6.1 GHz in Fig. 5(c) are due to repositioning of the antennas in between the $0.1 - 6.1$ and $6.0 - 12.0$ GHz measurement sessions, and are found to be almost exclusively due to a change of $\sigma_{S_{21}}^2(f)$ rather than $\tau_{S_{21}}(f)$.

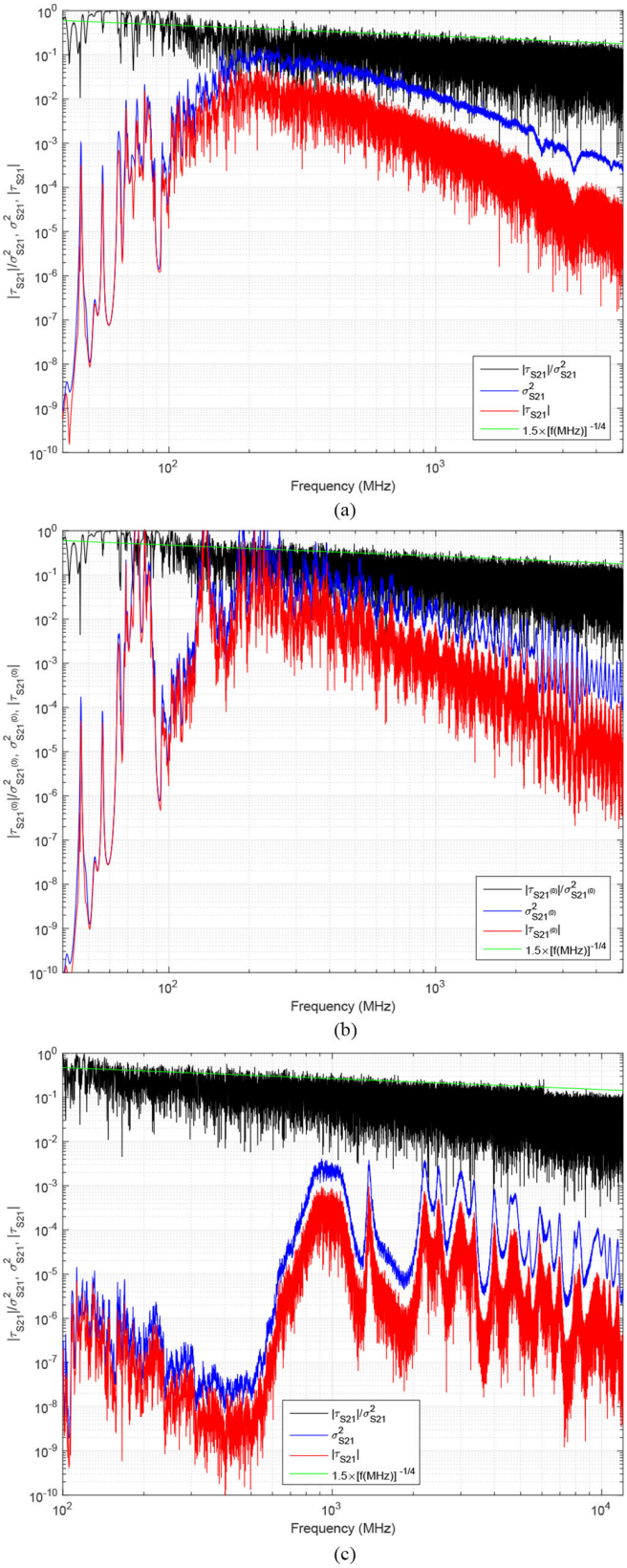

Fig. 5. Amplitude spectra of measured variance (blue), pseudovariance (red), and noncircularity quotient (black): (a) for raw $S_{21}(f)$ using identical log-periodic antennas; (b) for normalized transmission $S_{21}(f)/\{[1-S_{11}(f)][1-S_{22}(f)]\}$ using identical log-periodic antennas; and (c) for raw $S_{21}(f)$ using identical broadband dipole array antennas with different locations compared to (a) and (b).

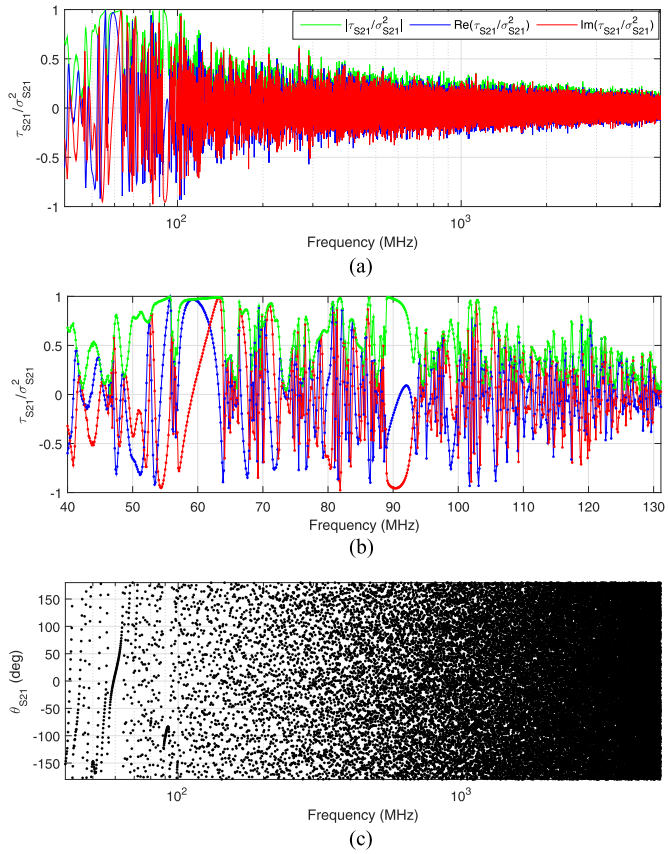

Fig. 6. (a) Spectra of $\varrho'_{S_{21}}$ (blue), $\varrho''_{S_{21}}$ (red), and $|\varrho_{S_{21}}|$ (green). (b) Close-up view of (a) from 40 MHz to $3f_{110}$. (c) Spectrum of $\arg(\varrho_{S_{21}})$.

(not shown). In combination with their envelopes decreasing and the NDoF increasing with frequency (cf., Section III-G), this suggests the possibility of a zero *mean* value $\varrho_{S_{21}}(f)=0$. However, as shown in Sections II-B2 and III-H, a substantial spread in the sampling PDF of $\varrho_{S_{21}}$, even for a zero ensemble average, still affects the sampling PDFs of U and Φ, thus increasing their uncertainty.

2) Polar Representation: Fig. 7 shows the polar[4] plot of $\varrho_{S_{21}}$ with parameter f. Values of $|\varrho_{S_{21}}|$ are close to their unity maximum value (unit circle) at low frequencies where the spectral variation of $\varrho_{S_{21}}$ is slow (e.g., near $f\sim 60$ MHz), corresponding to low values of $|S_{21}|$. As frequency and mode density increase, $\varrho_{S_{21}}(f)$ gyrates in an roughly spiral-like manner toward the center (ideal circularity). This spiraling indicates that $\varrho'_{S_{21}}$ and $\varrho''_{S_{21}}$ are strongly correlated quantities, reminiscent of earlier observations of *spatial* Cartesian scalar field components in the evaluation of planar field anisotropy and inhomogeneity [11, Figs. 5.5 and 7.1].[5]

[4]Each one of the 20001 data points in Fig. 7 is itself extracted from a 1000-point scatter plot of S_{21} at a particular frequency.

[5]The statistical I/Q anisotropy coefficient $(E'^2-E''^2)/(E'^2+E''^2)$ involves χ_1^2-distributed E'^2 and E''^2, unlike the (Cartesian polarization) field anisotropy coefficient $(|E_x|^2-|E_y|^2)/(|E_x|^2+|E_y|^2)$ [11, (21)], [10], which involves χ_2^2 distributed intensities. Hence for ideal circular fields, the statistical I/Q anisotropy is no longer uniformly distributed, as is the case for planar field anisotropy.

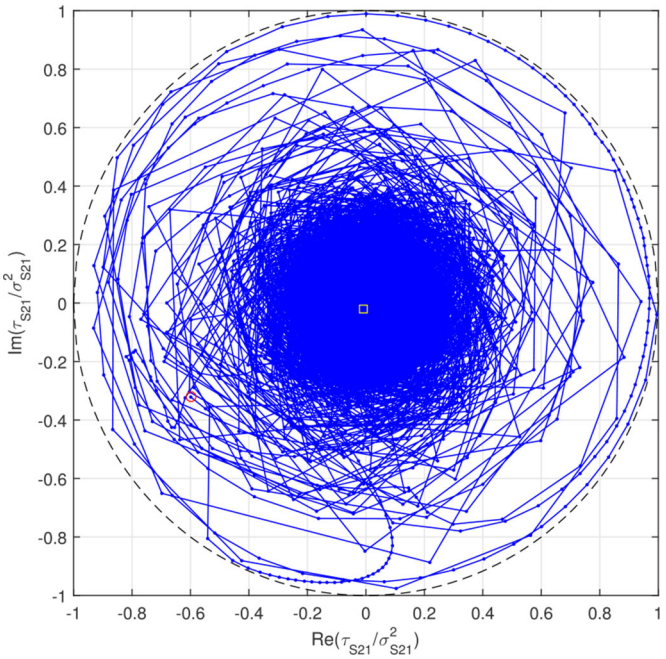

Fig. 7. Constellation diagram of $\varrho_{S_{21}}(f) \triangleq \tau_{S_{21}}(f))/\sigma^2_{S_{21}}(f)$ for 20 001 frequency points. Values $(-0.599, -0.321)$ at 40 MHz and $(-0.008, -0.021)$ at 5.040 GHz are indicated by a red circle and yellow square, respectively. Unit circle is shown as a visual aid only.

D. I/Q Correlation

1) Correlation Coefficient: The frequency characteristic of $\rho_{S'_{21},S''_{21}}(f) = \varrho''_{S_{21}}(f)/\sqrt{1-[\varrho'_{S_{21}}(f)]^2}$ (not shown) is almost indistinguishable from $\varrho''_E(f)$ in Fig. 6(a) with the same asymptotic spectral decay of its envelope, except at very low frequencies [$f < 100$ MHz; see Fig. 6(b)], where $\varrho'_{S_{21}}(f)$ differs substantially from zero.

2) Correlation Angle: Fig. 6(c) shows $\vartheta_{S_{21}}(f) = \tan^{-1}[\varrho''_{S_{21}}(f)/\varrho'_{S_{21}}(f)]$. The rapid approach toward a uniform distribution at all except the lowest frequencies confirms that a wide range of relative values of $\varrho''_{S_{21}}(f)$ and $\varrho'_{S_{21}}(f)$ occurs, positive as well as negative. Thus, complex noncircularity must be considered—including zero eccentricity (ellipticity) or zero correlation as special cases—as ensemble values or sample values of a corresponding sampling PDF of $R_{S_{21},S^*_{21}}$ for $\varrho_{S_{21}}$ (cf., Section II-B2).

E. Ellipticity: Eccentricity and Tilt

As indicated in Section II-B1, when the noncircularity arises as a perturbation from a circular complex symmetric (e.g., Gauss normal) PDF, this manifests itself as ellipticity. The equidensity ellipses of $f_{E',E''}$ are characterized by the axial ratio $\epsilon(f) \triangleq \sqrt{|\varrho_E(f)|}$ and tilt (orientation) $\alpha(f) \triangleq \vartheta_E/2$ [8]. Thus, on a logarithmic scale, $\epsilon(f)$ shows a similar frequency dependence as $|\varrho_{S_{21}}(f)|$ in Fig. 5(a), but now decreasing approximately as $f^{-1/8}$ (−2.5 dB/dec). Similarly, $\alpha(f)$ follows as halves of the values shown in Fig. 6(c). As noncircularity decreases with increasing frequency, the tilt becomes increasingly less relevant.

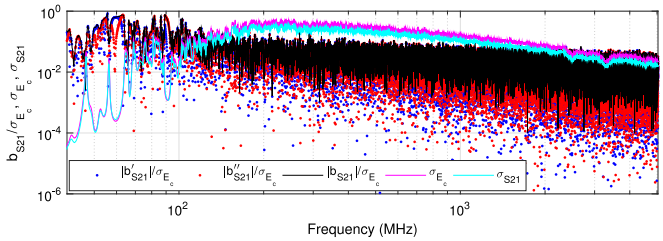

Fig. 8. Amplitude spectra of magnitudes of real and imaginary parts and modulus of $b_{S_{21}}/\sigma_{S_{21,c}}$, with associated standard deviation $\sigma_{S_{21,c}}$ of basis E_c. The measured $\sigma_{S_{21}}$ is shown for reference.

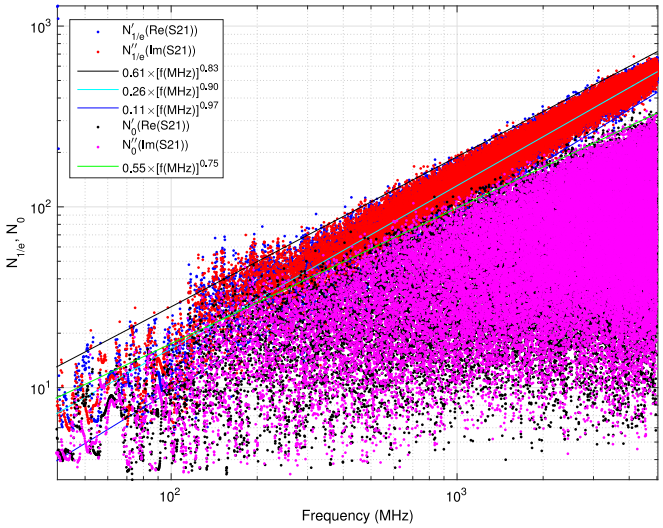

Fig. 9. Estimated number of independent stir states $N_x(f) = M/\ell_x(f)$ for two choices of threshold crossing level x for ACFs of S'_{21} and S''_{21}, with fitted asymptotic power-law models: (a) $N'^{(\prime)}_{1/e}(f)$ (blue and red dots); (b) $N'^{(\prime)}_0(f)$ (black and magenta dots).

F. WL Expansion Coefficients and Base Field

Fig. 8 shows the spectrum of the coefficient $b_{S_{21}}$ for the WL expansion of S_{21} and the standard deviation $\sigma_{S_{21,c}}$ for the associated circular $S_{21,c}$, as extracted from the data using (8). Because of the smallness of $|\varrho_{S_{21}}(f)|$, the perturbation to circularity is small, confirmed by the small values of $\sigma_{S_{21}}/\sigma_{E_c}$ and $b_{S_{21}}/\sigma_{S_{21,c}}$ close to $\varrho_{S_{21}}/2$ [compare with Fig. 6(a)].

G. Number of Independent Samples

Estimates of the number of independent stir states (NDoF) $N(f)$ are instrumental as a parameter in the sampling PDFs of U and Φ, as well as, e.g., in hypothesis testing for the statistical significance of circularity ($|\varrho_E| > 0$). Fig. 9 shows $N'^{(\prime)}_x(f)$ for two selected threshold levels, $x = 0$ and 1/e. The former yields true uncorrelation but is more sensitive to sample fluctuations and residual inhomogeneity, while the latter is a popular compromise level. The value of $N'^{(\prime)}_x$ can be estimated as $2\pi M/\ell_x(f)$, where $\ell_x(f)$ is the correlation length defined by the angular separation of the rotating mode stirrer for which the (sample) autocorrelation function (ACF) of $S'^{(\prime)}_{21}(\theta|f)$ crosses the threshold x upon linear interpolation. Large fluctuations in the sample

values of $N_0^{\prime(\prime)}(f)$ occur, even for small frequency changes. Increasing the threshold to 1/e yields a smaller range of fluctuation, but also inevitably higher estimates of $N_x^{\prime(\prime)}$ and, importantly, a higher rate of increase with frequency. A compromise value follows by extrapolating the values $\ell_{1/\mathrm{e}}^{\prime(\prime)}$ to the expected zero crossings $\ell_0^{\prime(\prime)\star}$ of the ensemble ACF $\mathrm{sinc}(\ell)$ for an ideal circular S_{21}, i.e., $\ell_0^{\prime(\prime)\star} = 1.429\ell_{1/\mathrm{e}}^{\prime(\prime)}$ and $N_0^{\prime(\prime)\star} = N_{1/\mathrm{e}}^{\prime(\prime)}/1.429$.

Whether a functional relationship between ℓ_0 and $|\varrho_E|$ exists that enables the latter to be used as threshold-free estimator of N, remains speculative. Based on their power-law envelope frequency dependencies, any such a relationship would be of the form $\ell_0 \propto |\varrho_E|^\kappa$ with $\kappa \simeq 3$.

H. Distributions: Empirical Versus Ensemble Versus Sampling PDFs, Elliptic Versus Circular Field

Fig. 10(a) shows a scatter plot for centered S_{21} data at $f_0 = 178.625$ MHz, measured using log-periodic antennas with listed values of the extracted eccentricity and tilt for an elliptic field model. For these data, Fig. 10(b) compares the empirical complementary cumulative distribution function (CCDF) against various theoretical CCDFs for $U \propto |S_{21}|^2$, i.e., $1 - F_U(u) \triangleq 1 - \int_0^u f_U(x)\mathrm{d}x$, for circular and elliptic ensemble and sampling PDF models. The sample noncircularity at this frequency ($r_{S_{21},S_{21}^*} = 0.505 + \mathrm{j}0.055$) causes considerable deviation of the elliptic ensemble (Bessel I) CCDF from the asymptotic circular (χ_2^2) CCDF, but is close to the circular sampling Bessel K CCDF for $N = 9.8$; see below. Significantly improved agreement[6] with the empirical CCDF is obtained by the elliptic sample CCDF (17) for $N = 9.8$. While excellent agreement exists in the "bulk" central part of the distribution ($0 \le u/\sigma_U < 2$), some discrepancy remains in the intermediate region $2 \le u/\sigma_U < 6$, where the heavier empirical tail suggests that some uncertainty remains unaccounted for, possibly because the distribution of N has not yet been included in the model (17), or because any statistical dependence between certain distribution parameters may be too strong.

At this relatively low f_0, the extracted estimates of N are small yet differ substantially ($N_0'(f_0) = 4.8$, $N_0''(f_0) = 11.5$, $N_{1/\mathrm{e}}'(f_0) = 32.7$, $N_{1/\mathrm{e}}''(f_0) = 25.4$). The best agreement between the empirical and theoretical elliptic sample CCDFs is found by fitting the latter to the former using N_0 as a free parameter. Based on minimization of the mean-square deviation between both CCDFs, this value is obtained as $N_0 = 9.8$. For this value of N_0, small-sample effects are considerable, as demonstrated by the much heavier tail of the empirical and elliptic sampling CCDFs compared to the elliptic ensemble CCDF. For the far tail region ($u/\sigma_U > 6$), the agreement is less but cannot be reasonably expected because $1 - F_U(u/\sigma_U > 6) < 0.02$ is of the order of the sampling resolution for the estimated N_0 and the stir set size ($N_0/M = 0.0098$), when statistical prowess becomes exhausted.

[6]Improved but slightly inferior agreement was also obtained for a circular sampling Bessel K CCDF with $N \simeq 2$, but this value is rather less plausible from Fig. 9 in this case.

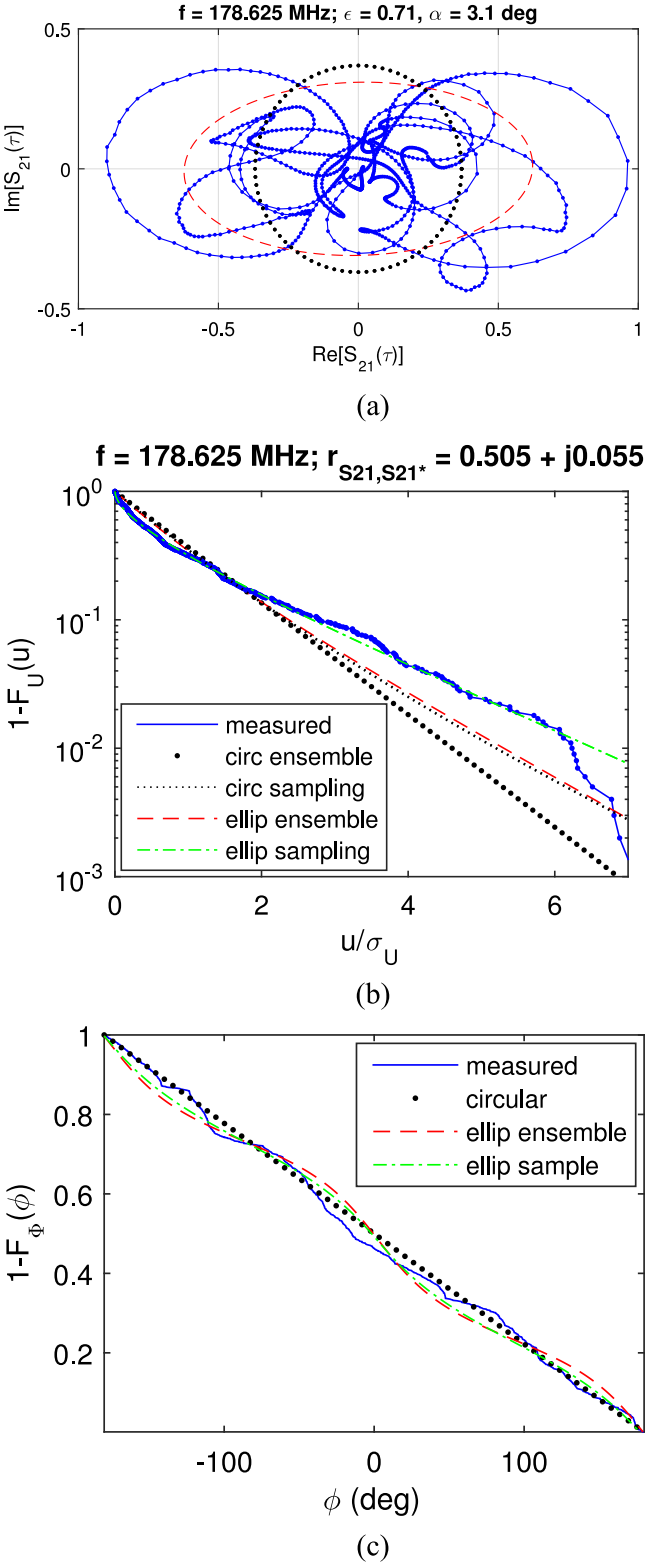

Fig. 10. (a) Scatter plot of measured data $S_{21}(\tau)$ at $f = 178.625$ MHz for 1000 stir states ($1 \le \tau \le 1000$). Asymptotic circular and extracted ensemble elliptic scatter models (shown with arbitrary scaling) are plotted for reference only. (b) CCDFs of intensity $|S_{21}|^2$: empirical (measured $|S_{21}|^2$), ideal circular ensemble (χ_2^2 CCDF), circular sampling (Bessel K CCDF with $N = 9.8$), elliptic ensemble ((10) with $|r_{S_{21},S_{21}^*}| = 0.508$), and elliptic sampling ((17) with $N = 9.8$). (c) CCDFs of phase $\arg(S_{21})$: empirical (measured $\arg(S_{21})$), circular ensemble or sampling (uniform CCDF), elliptic ensemble ((11) with $r_{S_{21},S_{21}^*} = 0.505 + \mathrm{j}0.055$), and elliptic sample ((25) with $N = 9.8$).

For Φ, Fig. 10(c) shows that ellipticity gives rise to undulations in its ensemble CCDF. These become damped in the sampling CCDF, where accounting for uncertainty of $\varrho_{S_{21}}$ is seen to yield a partial redistribution of phase toward uniformity. In general, the asymmetry of $1 - F_\Phi(\phi)$ with respect to the linear CCDF for a uniform Φ increases with increasing $|\varrho_{S_{21}}|$. Such departures from phase uniformity were already observed experimentally in [21, Fig. 22].

IV. Conclusion

In this paper, second-order statistics of in-phase and quadrature components of a quasi-random noncircular EM field were investigated and verified using data measured in a mode-stirred reverberation chamber. It was found that, typically, the statistical I/Q anisotropy (imbalance) and I/Q correlation are simultaneously nonzero and comparable in magnitude, except at very low frequencies (low modal overlap), where either quantity is nearly zero and where statistical modeling because inadequate. Thus, the pseudovariance and noncircularity quotient for reverberant fields are, in general, fully complex quantities. The I/Q imbalance and I/Q correlation show strong spectral fluctuations and a relatively slow spectral decay as $f^{-1/4}$. This rate of decay was found to be robust with respect to variable experimental conditions.

It was demonstrated how the expansion coefficients and variance of a circular basis field for a WL representation of a noncircular field can be extracted from measured S-parameter data. This WL expansion enables the extension of theorems and methods for time-harmonic fields to UWB fields, including digital modulated wireless signals.

The ensemble PDFs of the field intensity (energy, power density) and the associated I/Q phase for scalar elliptic fields were derived, with the noncircularity coefficient ϱ_E as a distribution parameter. For the PDF of the intensity, the anisotropy and correlation provide fully exchangeable contributions to $|\varrho_E|$. By contrast, the PDFs of the phase and phase-dependent energy $U|\Phi$ depend on both $|\varrho_E|$ and $\arg(\varrho_E)$. The increasing kurtosis observed in Fig. 3 for increasing ellipticity is similar to the phenomenon encountered in other models for imperfect circular reverberant fields and implies a higher probability of observing large values of the normalized energy or power, compared to predictions by simple ideal field models [21, Figs. 2 and 5]. Ellipticity further reinforces the effects of spatial anisotropy and inhomogeneity, in that it introduces additional physical parameters for the PDF of the I/Q field.

Sampling PDFs for noncircular normal fields with finite NDoFs extend the Bessel K sampling PDFs for circular fields. The elliptic sampling PDFs for energy and phase were compared against empirical distributions showing good qualitative and quantitative agreement. Sampling PDFs further increase the heaviness of the tails.

It is emphasized that considerable sample-to-sample and frequency-to-frequency variations of S_{21} data may exist, particularly at low frequencies and occasionally above $3f_{110}$ or near the "lowest usable frequency" [22], where $S_{21}(\tau|f)$ is better characterized by a closed and possibly self-intersecting random walk in the I/Q plane. Approximating the I/Q scatter plot by a uniformly filled ellipsoid constitutes a simple departure from a circular disk. Empirical CCDFs for $|S_{21}|^2$ tend to agree best with an elliptic ensemble or sampling CCDF when the scatter plot is (near-)symmetric about the origin. However, elliptic distributions are by no means universal at low frequencies or when losses are considerable. More sophisticated probabilistic models are then required. A proper test of hypothesis for ellipticity is, therefore, recommended prior to any parameter estimation and modeling of the data.

Appendix
Elliptic Fields, Energy and Phase for Imbalanced Cartesian Components

In $2p$-dimensional real space, an elliptic symmetric random electric (or magnetic) vector field $\underline{E}$ [23]–[25] has a stochastic representation of the form

$$\underline{E} = \underline{\mu}_E + \underline{\underline{\Sigma}}_E \cdot \underline{E}_s \tag{27}$$

where $\underline{\mu}_E$ is a constant vector (deterministic dc or line-of-sight field), $\underline{\underline{\Sigma}}_E$ is the Cholesky square root of the positive definite dispersion matrix $\underline{\underline{V}}_E \triangleq \underline{\underline{\Sigma}}_E \cdot \underline{\underline{\Sigma}}_E^T$, and $\underline{E}_s \triangleq R\underline{I}$ is a spherical random electric field, obtained as the product of a vector $\underline{I}$ uniformly distributed on the $2p$-dimensional unit sphere and a scalar nonnegative random generating variable R independent of $\underline{I}$. Different choices of R yield various classes of differently shaped and tailed PDFs for the $2p$-dimensional elliptic field (including Gauss normal, Student t, Bessel K, etc.) as

$$f_{\underline{E}}(\underline{e}) = \sqrt{\det(\underline{\underline{V}}_E^{-1})}\, g_R\left((\underline{e} - \underline{\mu}_E)^T \cdot \underline{\underline{V}}_E^{-1} \cdot (\underline{e} - \underline{\mu}_E)\right) \tag{28}$$

where the generator function for the PDF is defined by

$$g_R(r) \triangleq \frac{\Gamma(p)}{2\pi^p} \frac{f_R(\sqrt{r})}{(\sqrt{r})^{p-1}} \tag{29}$$

in which $f_R(\cdot)$ denotes the PDF of R. Asymmetric elliptic distributions (e.g., skewed and metadistributions) and their generalizations have also been defined and investigated.

Focusing on complex elliptic symmetric distributions [26] in the complex plane as a 2-D real space, let $E \equiv E' + \mathrm{j}E''$ and E^* represent a scalar elliptic-centered Gaussian random field and its complex conjugate, with sample values e and e^*. Based on a general form for their joint PDF that incorporates possible correlation between E' and E'' [27, eqs. (36)–(41)]

$$f_{\underline{Z}}(\underline{z}) = \frac{1}{\pi(\det \underline{\underline{V}})^{1/2}} \exp\left(-\frac{1}{2}\underline{z}^\dagger \cdot \underline{\underline{V}}^{-1} \cdot \underline{z}\right) \tag{30}$$

where

$$\underline{Z} = [E \quad E^*]^T, \qquad \underline{z} = [e \quad e^*]^T \tag{31}$$

$$\begin{aligned}\det \underline{\underline{V}} &= \langle E \cdot E^* \rangle^2 - \langle E \cdot E \rangle \langle E^* \cdot E^* \rangle \\ &= \sigma_E^4 - |\tau_E|^2 = 4\sigma_{E'}^2 \sigma_{E''}^2 (1 - \rho_{E',E''}^2)\end{aligned} \tag{32}$$

$$\underline{\underline{V}}^{-1} = \frac{1}{\det \underline{\underline{V}}} \begin{pmatrix} \sigma_E^2 & -\tau_E \\ -\tau_E^* & \sigma_E^2 \end{pmatrix}. \tag{33}$$

Substitution yields

$$\begin{aligned}f_{E,E^*}(e,e^*) = &\frac{1}{\pi \sigma_E^2 \sqrt{1 - |\varrho_E|^2}} \\ &\times \exp\left[-\frac{e \cdot e^* - [(e^*)^2 \varrho_E + e^2 \varrho_E^*]/2}{\sigma_E^2 (1 - |\varrho_E|^2)} \right]\end{aligned} \tag{34}$$

where $\varrho_E \stackrel{\Delta}{=} \tau_E / \sigma_E^2$. With the polar representations $e = \sqrt{|e|^2} \exp(\mathrm{j}\phi)$ and $\varrho_E = |\varrho_E| \exp(\mathrm{j}\vartheta_E)$, this is rewritten as

$$\begin{aligned}f_{E,E^*}(e,e^*) = \; f_{|E|^2,\Phi}(|e|^2,\phi) = &\frac{1}{\pi \sigma_E^2 \sqrt{1 - |\varrho_E|^2}} \\ &\times \exp\left[-\frac{1 - |\varrho_E| \cos(2\phi - \vartheta_E)}{\sigma_E^2 (1 - |\varrho_E|^2)} e \cdot e^* \right].\end{aligned} \tag{35}$$

Here, $f_{E,E^*}(e,e^*)$ coincides with $f_{|E|^2,\Phi}(|e|^2,\phi)$ because $|\det[\partial(e,e^*)/\partial(|e|^2,\phi)]| = 1$ for the variate transformation from E and E^* to $|E|^2$ and $\Phi = \tan^{-1}(E''/E')$. Using [15, eq. (3.915.4)], the marginal PDFs of the field intensity (energy, power) $|E|^2$ and the phase angle Φ follow as

$$f_{|E|^2}(|e|^2) = \int_0^{2\pi} f_{|E|^2,\Phi}(|e|^2,\phi) \mathrm{d}\phi \tag{36}$$

$$= \frac{\exp\left[-\frac{|e|^2}{\sigma_E^2 (1 - |\varrho_E|^2)} \right]}{\sigma_E^2 \sqrt{1 - |\varrho_E|^2}} I_0\left(\frac{|\varrho_E||e|^2}{\sigma_E^2 (1 - |\varrho_E|^2)} \right) \tag{37}$$

$$f_\Phi(\phi) = \int_0^\infty f_{|E|^2,\Phi}(|e|^2,\phi) \mathrm{d}|e|^2 \tag{38}$$

$$= \frac{\sqrt{1 - |\varrho_E|^2}}{2\pi \left[1 - |\varrho_E| \cos(2\phi - \vartheta_E)\right]} \tag{39}$$

for $0 \le |e|^2 < +\infty$ and $-\pi \le \phi < +\pi$, respectively, where $I_0(\cdot)$ is a modified Bessel function. The PDF (37) has been previously obtained for real ϱ_E in a different context and formalism (effective quantum Hamiltonian) [28]–[30]. The corresponding phase PDF (39) completes the stochastic characterization of E and is a generalization of the special case of equivariance, obtained in [5] with a different phase reference. The generality of the present derivation does not limit its application to cavities nor to a distinction between standing and traveling waves as in [28], because the random field is solely characterized by its *local* statistical I/Q imbalance, correlation, and variance.

The PDF $f_{|E|^2}(|e|^2)$ is independent of ϑ_E because of the periodicity of the cosine function and full period of integration. If, however, the ranges of Φ and/or $|E|^2$ are restricted (e.g., at relatively low frequencies, when Ohmic losses or leakage are present,[7] or when the stir range is limited), then this affects the limits of the integration in (36) and (38) and hence (37) and (39). The locations of the two maxima of $f_\Phi(\phi)$ coincide with a coordinate axis (canonical ellipse) if I and Q are uncorrelated ($\vartheta_E = 0$). The height of these maxima increases with increasing I/Q statistical anisotropy ϱ_E'.

Expressions (37) and (39) define simple multiplicator functions $g(|\varrho_E|)$ and $h(\varrho_E)$ for the ideal circular χ_2^2 PDF $f_{|E|^2}(|e|^2) = \exp(-|e|^2/\sigma_E^2)/\sigma_E^2$ and uniform PDF $f_\Phi(\phi) = (2\pi)^{-1}$, respectively. Compared to these reference PDFs, g produces increased kurtosis, while h induces two increasingly pronounced peaks, at $\phi_1 = \vartheta_E/2$ and $\phi_2 = \vartheta_E/2 + \pi$.

ACKNOWLEDGMENT

S-parameter measurements were performed at the Institute of Electronics and Telecommunications Research of the National Institute of Applied Sciences, Rennes, France.

REFERENCES

[1] J. G. Kostas and B. Boverie, "Statistical model for a mode-stirred chamber," *IEEE Trans. Electromagn. Compat.,* vol. 33, no. 4, pp. 366–370, Nov. 1991.

[2] L. R. Arnaut, "Probability distributions of random electromagnetic fields in the presence of a semi-infinite isotropic medium," *Radio Sci.,* vol. 42, p. RS3001, 2007.

[3] J. A. Russer and P. Russer, "An efficient method for computer aided analysis of noisy electromagnetic fields," in *Proc. IEEE Int. Microw. Symp.*, Jun. 2011, pp. 1–4.

[4] L. R. Arnaut and C. S. Obiekezie, "Stochastic analysis of wideband near-field emissions from dipole antennas and integrated circuits," *IEEE Trans. Electromagn. Compat.,*vol. 56, no. 1, pp. 93–101, Feb. 2014.

[5] R. Serra and F. Canavero, "Bivariate statistical approach to 'good-but-imperfect' electromagnetic reverberation," *IEEE Trans. Electromagn. Compat.,*vol. 53, no. 3, pp. 554–561, Aug. 2011.

[6] P. Bello, "Correlation functions in a tapped delay line model of the orbital dipole channel," *IEEE Trans. Inf. Theory,*vol. 9, no. 1, pp. 2–11, Jan. 1963.

[7] F. D. Neeser and J. L. Massey, "Proper complex random processes with applications to information theory," *IEEE Trans. Inf. Theory,*vol. 39, no. 4, pp. 1293–1302, Jul. 1993.

[8] E. Ollila, "On the circularity of a complex random variable," *IEEE Signal Process. Lett.,* vol. 15, pp. 841–844, Nov. 2008.

[9] O. Lobkis and R. Weaver, "Complex modes in a reverberant dissipative body," *J. Acoust. Soc. Am.,* vol. 108, pp. 1480–1485, 2000.

[10] L. R. Arnaut, "Field anisotropy, field inhomogeneity and polarization bias in imperfect reverberation chambers," NPL Tech. Note R981120, Nov. 1998.

[11] L. R. Arnaut and P. D. West, "Evaluation of the *NPL* untuned stadium reverberation chamber using mechanical and electronic stirring techniques," NPL Tech. Rep. CEM 11, Aug. 1998.

[12] S. A. van Langen, P. W. Brouwer, and C. W. J. Beenhakker, "Fluctuating phase rigidity for a quantum chaotic system with partially broken time-reversal symmetry," *Phys. Rev. E,* vol. 55, pp. R1–R4, Jan. 1997.

[13] B. Picinbono and P. Chevalier, "Widely linear estimation with complex data," *IEEE Trans. Signal Process.,* vol. 43, no. 8, pp. 2030–2033, Aug. 1995.

[14] K. Scherer, "Measurement tools for digital video transmission," *IEEE Trans. Broadcast.,*vol. 39, no. 4, pp. 250–263, Dec. 1993.

[15] I. S. Gradshteyn and I. M. Ryzhik, *Table of Integrals, Series, and Products,* 7th ed. Amsterdam, the Netherlands: Academic, 2007.

[16] L. R. Arnaut, "Sampling distributions of random electromagnetic fields in mesoscopic or dynamical systems," *Phys. Rev. E,* vol. 80, no. 3, p. 036601, 2009.

[7] These physical factors also affect $f_{E,E^*}(e,e^*)$.

[17] L. R. Arnaut, "Mode-stirred reverberation chambers: a paradigm for spatio-temporal complexity in dynamic electromagnetic environments," *Wave Motion,* vol. 51, no. 4, pp. 673–684, Jun. 2014.
[18] L. R. Arnaut, "Measurement uncertainty in reverberation chambers—I. Sample statistics," NPL Rep. TQE 2, 2nd ed., pp. 1–136, Dec. 2008.
[19] R. A. Fisher, "Frequency distribution of the values of the correlation coefficient in samples from an indefinitely large population," *Biometrika,* vol. 10, no. 4, pp. 507–521, 1915.
[20] L. R. Arnaut, M. I. Andries, J. Sol, and P. Besnier, "Evaluation method for the probability distribution of the quality factor of mode-stirred reverberation chambers," *IEEE Trans. Antennas Propag.,*vol. 62, no. 8, pp. 4199–4208, Aug. 2014.
[21] L. R. Arnaut, "Limit distributions for imperfect electromagnetic reverberation," *IEEE Trans. Electromagn. Compat.,*vol. 45, no. 2, pp. 357–377, May 2003.
[22] *Electromagnetic Compatibility (EMC). Part 4: Testing and Measurement Techniques: Section 21: Reverberation Chambers,*International Electrotechnical Commission, 2nd ed., IEC 61000-4-21, Geneva, Switzerland, Jan. 2011.
[23] D. K. McGraw and J. F. Wagner, "Elliptically symmetric distributions," *IEEE Trans. Inf. Theory,*vol. 14, no. 1, pp. 110–120, Jan. 1968.
[24] D. Kelker, "Distribution theory of spherical distributions and a location-scale parameter generalization," *Sankhyā, A,* vol. 32, pp. 419–430, 1970.
[25] S. Cambanis, S. Huang, and G. Simons, "On the theory of elliptically contoured distributions," *J. Multivariate Analysis,* vol. 11, pp. 368–385, 1981.
[26] P. R. Krishnaiah and J. Lin, "Complex elliptically symmetric distributions," *Commun. Stat., Theory Methods,*vol. 15, no. 12, pp. 3693–3718, 1986.
[27] A. van den Bos, 'The multivariate complex normal distribution—A generalization," *IEEE Trans. Inf. Theory,*vol. 41, no. 2, pp. 537–539, Mar. 1995.
[28] R. Pnini and B. Shapiro, "Intensity fluctuations in closed and open systems," *Phys. Rev. E,* vol. 54, no. 2, pp. R1032–R1035, Aug. 1996.
[29] K. Zyczkowski and G. Lenz, "Eigenvector statistics for the transitions from the orthogonal to the unitary ensemble," *Z. Physik B,*vol. 82, no. 2, pp. 299–303, 1991.
[30] P. W. Brouwer, "Wave function statistics in open chaotic billiards," *Phys. Rev. E,* vol. 68, no. 4, p. 046205, 2003.

Luk R. Arnaut received the Graduate degree from the University of Ghent, Ghent, Belgium, and the M.Sc. and Ph.D. degrees in electronic engineering from the University of Manchester (UMIST), Manchester, U.K.

He was a Research Associate with UMIST, including secondments to the Defense Research Agency (QinetiQ) and the Naval Research Laboratory, Washington DC, USA, involved with theoretical simulation and experimental work on chiral metamaterials. During 1995–1996, he was a Technical Consultant with BAE Systems for its RUSSTECH program. In 1996, he joined the U.K. National Physical Laboratory, working on resonators, metasurfaces, EMC, and antennas, becoming Lead Scientist of the Wireless Communications Group. In 2010, he founded AKS, Ltd., providing technical and scientific consultancy to engineering and finance businesses. In 2012, he joined the University of Nottingham, leading its research effort on stochastic characterization of near-field radiated emissions. Since 2014, he has been with the Queen Mary University London, London, U.K., heading the Laboratory of Stochastic Electromagnetism and Wave Complexity. He has served as Chairman of IEC Joint Task Force CISPR/A-SC77B on reverberation chambers and is a Member of various international working groups, steering committees, and advisory boards. He has been a Visiting Professor at Imperial College London, London, the French National Institute of Applied Sciences (INSA), Rennes, France, and the University of Paris, Paris, France. He is the principal author of more than 150 papers and reports, and holds two patents.

Dr. Arnaut received the Rayleigh Prize and the IEC 1902 Award. He is a Fellow of IET, London.